Draft version August 30, 2025

Typeset using LaTeX **twocolumn** style in AASTeX631

Searching for Globular Clusters in NGC 7332 and NGC 7339

Heather Lenz, Dr. Langill, and Dr. Taylor

ABSTRACT

This project aims to locate globular clusters (GCs) orbiting NGC 7332 and NGC 7339 and investigate the potential for galactic interaction. Data from the u, i, and K_s filters was used to construct a colour colour diagram to locate the GCs as described by Muñoz et al. (2014). Archival u and i band data was obtained from the Canadian Astronomy Data Center taken by the MegaCam instrument on the Canada-France-Hawaii Telescope (CFHT). CFHT's WIRCam instrument collected the K_s band data due to a proposal written as part of SCIE 507 global learning class during spring 2024 led by Dr. Langill and Dr. Taylor. CFHT images were combined using the Mira software, and photometric data was measured using Source-Extractor. Using the colours $(u-i)_0$ and $(i-K_s)_0$ a colour-colour diagram was constructed from which 90 GC candidates where identified. The coordinates of the GC candidates were then used to study possible galactic interaction by creating density plots.

1. INTRODUCTION

Groups of hundreds of thousands of stars, called globular clusters (GCs), have been found orbiting nearly every galaxy. Much about GC formation and its role in galactic evolution is not fully understood. Studying globular clusters provides insights into galaxy formation, star formation, galactic interaction, evolution, and dark matter distribution. Colour colour diagrams have been shown to be the best method to identify GCs, these diagrams are created with three filters such as BVR, gzK_s, and uiK_s. The uiK_s diagram using the colours $(u-i)_0$ and $(i-K_s)_0$, Fig.4, was shown by Muñoz et al. (2014) to be the most effective in separating the GCs from background galaxies and foreground stars. Therefore for this project a uiK_s diagram was created to locate the GCs around the galaxies NGC 7332 and NGC 7339. The possible interaction of these galaxies will then be investigated through the distribution of GCs.

The galaxies NGC 7332 and NGC 7339 located in the constellation Pegasus were chosen primary as the Canadian Astronomy Data Center (CADC) contained data from the Canada France Hawaii Telescope (CFHT) in the u and i filters but not the K_s. Therefore we were able to write a proposal to gather the K_s band data using

CFHT's WIRCam instrument. Additionaly the edge-on orientation of both galaxies minimizes the extinction of GCs by the galactic disk, allowing for a more accurate assessment of their spatial distribution and properties.

Specific frequency, S_N, is an effective way to describe the GC system around a host galaxy. First described by Harris & van den Bergh (1981) S_N is a measure the total number of GCs normalized to the host galaxies luminosity, defined by the fallowing equation:

$$S_N = N_{GC} 10^{0.4(M_V+15)} \quad (1)$$

(Harris & van den Bergh (1981)), in Eq.1 N_{GC} is the total number of GCs, M_V is the host galaxy absolute V band magnitude. The S_N calculated for one galaxy can be used for another as long as they have the same mass-to-light (M/L) ratios Brodie & Strader (2006). From Young et al. (2012) for NGC 7332 $S_N = 0.9 \pm 0.3$, $M_V = -20.7$ and for NGC 7339 $S_N = 0.5 \pm 0.2$, $M_V = -20.4$. Thus using Eq.1 the number of expected GCs is $N_{GC} = 175 \pm 15$ for NGC 7332 and $N_{GC} = 75 \pm 10$ for NGC 7339. The high expected number of GCs around these galaxies makes them ideal candidates for our study.

2. THE DATA

The data from CFHT was used to create a uiK_s diagram to identify GCs. The uiK_s filters are spread out over the electromagnetic spectrum their wavelengths are u 311-397nm near-UV Bertin (2024), i 699-854nm in optical, and K_s 1983-2308nm near-IR Barrick (2024). The u and i filter data was gathered from the CADC, which was taken by CFHT's MegaCam instrument. The CADC contained 7 u band images with a 700 second exposure time observed in 2014 and 6 i band images with a exposure time of 119 seconds observed in 2009. The K_s filter data was taken by CFHT's WIRCam instrument. The K_s band data was taken as a result of a Directors Discretionary Time (DDT) proposal to CFHT as part of a global learning class (SCIE 507) organized by Dr. Langill and Dr. Taylor in May 2024. From this proposal 163 images of 20 second exposures each using WIRCam were collected.

I was a member of 12 undergraduate students in this class who had the incredible opportunity to write proposals for both Gemini North Telescope and CFHT. The proposal to CFHT was successful however Gemini North were unable to take our data. During the class we toured the base the base facilities in Hawaii of both telescopes where we presented our proposals to the scientists that worked there, attended talks about the telescopes, the various instruments, how observing schedules are made and how they control the telescopes. We also had the amazing opportunity to tour the telescopes at the summit of Maunakea.

3. DATA REDUCTION

The data reduction process can be divided into three main parts: image pre-processing done by CFHT, image stacking using Mira, and image calibration.

3.1. *Image Pre-Processing*

The raw data from CFHT was pre-processed though the 'I'iwi pipeline, version 2.0.[1] This process has five steps, flagging saturated pixels, nonlinearity correction, dark subtraction, flat-fielding, and bad-pixel masking creating the images seen in Fig.1. First pixels with a threshold value of 36,000 ADU in the raw images were identified Muñoz et al. (2014). This locates the likely saturated pixels and keeps a record of them. In the pre-processed image these saturated pixels were flagged with the value 65535 ADU. The flux response of IR detectors are infamously non-linear, WIRCam being no exception with around 5% non-linearity at 30,000 ADU. This was corrected for using non-linearity modelling with the WIRCam sensor. At the beginning and end of each observing night at CFHT darks and Twilight flats are taken, from which the master dark and flat are computed and applied to the images. However since the dark current of the WIRCam detector is low, less than 1 e^{-}/sec the dark subtraction has negligible effect on the pre-processed image. A master bad-pixel mask is created by analyzing the master flats identifying bad pixels though a sigma-threshold algorithm. The bad-pixel mask is constructed such that good pixels are given a value of 1 and bad pixels a value of 0. The final pre-processed images are as seen in Fig.1

[1] https://www.cfht.hawaii.edu/Instruments/Imaging/WIRCam/IiwiVersion2Doc.html

3.2. *Image Stacking*

Initially, to stack the pre-processed images the programs Source-Extractor, Scamp, and SWarp where used. However, the stacked images did not yield sufficient sources with u, i, and K_s magnitudes to create a uiK_s diagram. To successfully stack the images Mira a image processing and analysis software was used.

3.2.1. *Source-Extractor, Scamp, and SWarp*

To process the data from CFHT the first strategy involved three programs, Source-Extractor (SE) Bertin & Arnouts (1996), Scamp Bertin (2006), and SWarp Bertin et al. (2002). First SE is builds a catalogue containing photometric data on all sources in each pre-processed images from CFHT. SE measures sources RA/Dec, magnitude, flux, ellipticity, etc. The program Scamp then compares the catalogues SE built to the Two Micron All Sky Survey (2MASS) Skrutskie et al. (2006). Scamp then calculates how much each image needs to be shifted to match 2MASS by measuring the distance between the same source in the two catalogues. Several check plots were made to show how well the images are lined up with eachother and 2MASS. The input settings of SE and Scamp where optimized using the check plots to be well align the images. SWarp is then run to shift and stack the FITS images together based on Scamp's calculation. However, problems arose as the final stacked images contained artifacts which affect the final photometry. This effect was minimized by changing

the stacking settings used by swarp such as BACK_SIZE and BACK_FILTERSIZE which change how the image is stacked. This process was ran for each filter to create a final u, i, and K_s image. SE was then run on the three final images, to create a catalogue of source magnitudes and RA/Dec across three filters which is used to construct the uiK_s diagram. However when matching the source catalogues together, described in section 5, not enough matches were found to construct a uiK_s diagram indicating errors in the alignment of the images. After checking the FITS file headers, python code to run the programs, and changing the input parameters for the programs, these problems persisted. These issues lead to use Mira to stack the images instead.

3.3. *Image stacking with Mira*

The pre-processed images from CFHT were successfully stacked using Mira Mirametrics (2024). For Mira to be able to process the images, the chips in each of the images needed to be separated. Each WIRCam image is made up of 4 chips and each MegaCam image made of 36 chips. To make the final images all 4 of WIRCam's chips were staked together and because of time constraints only 2 out of the 36 chip's images were stacked to create the u and i final images, as they were the only ones imaging the galaxies. To stack the separated images in Mira there are five steps, sort images into subsets, stack images in each subset together, apply a pixel mask to the subsets, stack subsets from each chip together, and stack the chips together. For this explanation I will be referencing the K_s band data however the processing is the same for the u and i bands.

3.3.1. *Creating Subsets*

Due to the dithering patterns of CFHT during the observation, Fig.2, stacking the images taken at the same location first and then stacking the subsets together is the most effective strategy. Creating the subsets involved taking all images separated from each chip and identifying groups of images where the galaxies appeared at the same location.

3.3.2. *Stacking Together the Images in each Subset*

To stack each subset's images together the alignment must be perfected using registration. Mira's registration toolbar was used, which enables the selection of the same stars across the images in the set. Once the stars are selected Mira then calculates the required shift/shear needed to line up the centroids. Note that shifting the image only translates the image vertically/horizontally where shearing the image will stretch and rotate the image. Mira is then used to combine the image set using the Mean Masked by 0 method which calculates the counts in the final image using Eq.2:

$$C_{MM0} = \frac{1}{n}\sum_{i=1}^{n} c_i \quad \text{if} \quad c_i \neq 0 \tag{2}$$

This equation creates a final image based on the mean value of each pixel across the registered subset except if the pixel have a value of zero. If a pixel has a value of

zero it is not included in the mean calculation thus does not negatively effect our final image. The patches of zeros, as seen in Fig.1, are a part of the bad-pixel masking during the image pre-processing stage as discussed in section 3.1.

3.3.3. *Pixel Masking*

In order to combine the subsets and not have negative effects from the large patches of zeros lowering the mean value for a pixel, a pixel mask was used. The pixel mask was used to change all the pixels in a image with a value of zero and replace them with the average background value. A combined image of the chip's subsets was created using a minimum combine method, which selects the smallest pixel value from each corresponding pixel location. The minimum combined image highlighted the patches of zeros on the chip leaving the rest of the image the lowest background value because of dithering. A pixel mask was then created on the minimum combined image which identified the location of every pixel with a value of zero. This pixel mask was then applied to every stacked subset and replaced every pixel with a value of zero with the average background value. Note that this step was only applied to the K_s band image stacking as the MegaCam instrument did not have patches of zeros. However, chips of the u and i images had borders with values of -0.004 or 0.004 which were negatively affecting the mean combined image. To compensate for this issue these chips cropped to remove these nonsensical values.

3.3.4. *Creating the final image*

With the images in each subset combined and pixel masked the final image for chip can be created. The final images from each chip can then be combined together to create the final image. Dithering the observations shifts each subset relative to the galaxies. Accurate image registration, as described in Section 3.3.2, is essential for successful stacking.

The registration process in Mira was done in two steps first to get the images roughly lined up, and second to make sure the images are precisely lined up. To roughly line up the images using Mira's registration toolbar one star was selected that appeared in every image, the required transformation was calculated to line up this point by shifting the image only. To precisely line up the image the same registration tool bar however many stars were selected that appeared in each image. Then Mira calculated the required transformation to line up the stars using the shear method which allows for image rotation, shift, and stretch.

Now that all the subsets for each chip are aligned with each other they can be stacked together to create the final image for that chip, using the same mean masked by zero described in section 3.3.2. These steps in the mira processing are then repeated on every chip such that, for each filter to create the final stacked u, i, and K_s as seen in Fig.3.

4. IMAGE CALIBRATION

In order to use Source-Extractor (SE) to perform photometry on the data each image needs to be RA/Dec and zero point calibrated. To RA/Dec calibrate the images we use the World Coordinate System (WCS) that defines the agreed upon locations objects in the sky. To calibrate the zero point for this data, point sources were found in the Simbad database Wenger et al. (2000) are used by Mira to calculate the zero point which is then used by SE.

4.1. *RA/Dec Calibration*

To RA/Dec calibrate the images to the World Coordinate System (WCS) the fully stacked images were uploaded to Astrometry.net[2] Lang et al. (2012) which edits the image to have the same scale, pointing, and orientation according to the WCS information. To do this Astrometry.net first detects the stars in the image, then compares the detected stars to index files to generate a hypotheses of the images astrometric calibration. To test this hypothesis Astrometry.net uses Bayesian decision theory, when the hypothesis passes the image then is returned to the user with the astrometric calibration. If the hypothesis does not pass this test a new one is created by searching though the index files. The success rate for the calibration is >99.9% for near UV and visual imaging survey data Lang et al. (2012).

[2] See https://nova.astrometry.net/upload

4.2. *Zero point Calibration*

The zero point of a image describes the needed offset to match the measured magnitudes to catalogue values, for this project Simbad Wenger et al. (2000) was used to find these values. To calculate the zero point, point sources found in Simbad, with u, i, or K_s magnitudes, were added as standard stars in Mira. Mira then compares the magnitude it measures the star at and the catalogue's magnitude to calculate the zero point. For the u band image 7 quasars were used, for the i band image 6 quasars, and the K_s band image 20 stars. The standard stars used to calibrate the images were found in Simbad from the Sloan Digital Sky Survey (SDSS) Albareti et al. (2017), Gaia Gaia Collaboration et al. (2023), Tycho Catalogue (TYC) Wicenec (1997), Two Micron All Sky Survey (2MASS) Skrutskie et al. (2006). The results of this calibration can be found in Table 1 which shows the zero point calculated by Mira to be around a degree lower than given by CFHT. In order for Source-Extractor to perform accurate photometry on the images they need to be zero point calibrated such that the airmass and airmass term for each filter/instrument is taken into account as seen in Eq.3:

$$ZP_{SE} = ZP_{Mira} + 1.85 + AT(AM_{avg}) \tag{3}$$

ZP_{SE} is the zero point given to Source-Extractor to do photometry on every source. ZP_{Mira} is the zero point Mira has calculated using the standard stars, AT is the airmass term as defined by the CFHT website for each

filter, AT_{avg} is the average airmass over the observation period. The value of 1.85 has to be added in order to convert the Vega magnitudes used by Mira to AB magnitudes used by SE. Since the three zero points given to SE are all calibrated to catalogue values this means the photometry will be able to differentiate the GCs though the uiK_s diagram.

5. PHOTOMETRY WITH SOURCE-EXTRACTOR

SExtractor (*source-extractor*/SE) Bertin & Arnouts (1996) is a program that is used to build catalogues of objects in an astronomical images. SE was used in this project to build three catalogues one for each of the final stacked and calibrated images. When SE is run on a image it is linked to a configuration file containing all relevant instrument configuration information (gain, pixel scale, read noise, etc) for WIRCam[3] or Megacam[4] along with SE settings and output parameters. SE outputs a catalogue containing the RA/Dec (J2000), magnitude, flux radius, etc of every source in the image. The error in SE's measured magnitudes is shown in Fig.15 where the error is ~ 0 for sources with low magnitudes. The photometry data contained in these catalogues will be used to differentiate background galaxies, foreground stars, and globular clusters.

[3] https://www.cfht.hawaii.edu/Instruments/Imaging/WIRCam/quickinformation.html

[4] https://www.cfht.hawaii.edu/Instruments/Imaging/Megacam/generalinformation.html

A software called Topcat Taylor (2011) is then used to match the RA/Dec of sources present in each of the three SE catalogues for the u, i, and K_s filters. The aim is to build a combined (matched) catalogue made up of only sources that have a measured magnitude in all filters. This was done by first matching the u and i catalogues where 4771 pairs were found, then matching that catalogue with K_s where 1928 pairs were found. Therefore a catalogue of 1928 sources with a u, i, and K_s magnitude was created.

6. THE UIK_S DIAGRAM

The uiK_s diagram as shown in Fig.4, is based on near-UV, optical, and near-IR (u, i, K_s) photometry providing an efficient method to separate GCs, stars, and galaxies Muñoz et al. (2014). The diagram work similarly to a Hertzsprung–Russell (HR) diagram which separates classes of stars based on their $B-V$ colour and intrinsic brightness, essentially sorting stars by their temperature and magnitude. The uiK_s diagram works by separating different objects made of star based on their $(u-i)_0$ and $(i-K_s)_0$ colours. Background galaxies are found in the upper portion of the plot, with younger star forming galaxies on the left, and older passive towards the right. The trend of star formation in background galaxies is because of the increased $H\alpha$ emission, which is closest to the i band, in galaxies forming stars. This trend also causes the GCs to be separated from the galaxies as they are non star forming objects.

Main sequence (MS) stars are located near the bottom of the diagram organized by MS turn-off stars which are hotter/bluer on the left to lower-MS stars which are cooler/redder on the right Muñoz et al. (2014). A stars temperature is intrinsically related to its colour showing how the colour colour diagram can be thought of as temperature temperature diagram Taylor et al. (2017). This shows why GCs are separated from the main sequence stars displayed on the plot. Therefore demonstrating how GCs can be distinguished in the uiK_s diagram.

To correct for Milky Way dust extinction, the measured magnitudes are normalized. This involves accounting for the preferential absorption of blue (u/i) light compared to near-IR (K_s) light. The NASA/IPAC Extragalactic Database (NED)[5] Helou et al. (1991) was used to find the magnitude offsets needed to normalize each filter while observing the RA/Dec of these two galaxies. Magnitudes were corrected by subtracting 0.158 for the u filter, 0.063 for the i filter, and 0.014 for the K_s filter.

To create a uiK_s diagram using the photometry done with source-extractor using the matched catalogue from Topcat, the u, i, and K_s magnitudes were normalized, then subtracted to find the values of the colours $(u-i)_0$ and $(i-K_s)_0$ for each point, then were plotted as seen in Fig.6.

[5] https://ned.ipac.caltech.edu/extinction_calculator

7. FILTERING GLOBULAR CLUSTERS

To identify possible GC candidates sources were selected corresponding to the location in the uiK_s diagram of GCs as discussed by Muñoz et al. (2014) as shown in Fig.6. This meant out of the 1928 matched sources in Fig.5, 282 were initially selected as possible GC candidates. To filter the GC candidates, cutouts of the i band image were made 10" around the RA/Dec coordinates of each candidate. These cutouts were then used to sort out candidates that were more likely GCs based on their ellipticity. Cutouts with well defined, round sources, Fig.7, were isolated as GC candidates while cutouts that showed fuzzy elliptical objects, Fig.8, were taken out. This processed narrowed the GC candidates from 282 to 90.

8. GLOBULAR CLUSTERS DENSITY ANALYSIS

To investigate the potential gravitational interaction between NGC 7332 and NGC 7339, the spatial distribution (RA/Dec) of the identified GC candidates was studied. Due to time limitations, three different methods were used to generate density colour plots using Python. The first method was using a python package from SciPy Virtanen et al. (2020) called scipy.stats. A density plot Fig.12 was created using scipy.stats which is used to study two numerical variables in a plotting area. In this case the two numeric variables are for the positions of the GC candidates ALPHA_J2000 (RA) and DELTA_J2000 (Dec) both in units of degrees. The pack-

age calculates a 2D kernel density estimate by dividing the plot into 300 bins per axis. Each GC candidate adds weight to a specific bin. The density plot then displays a Gaussian curve fitted to the bin weights using a colour gradient. The second method was using the Seaborn Waskom et al. (2017) Python package which analyzes the data using similar except with more display options. In the Seaborn package density can be displayed with a colour gradient or shown as a topographic map as shown in Fig.13. The third method I used to show GC density also used the Seaborn package except splitting the image into 30 bins per axis and displays using a bar graph the number of GC candidates in each bin Fig.14.

Analyzing the three density graphs they all show a large concentration of GC candidates around NGC 7339 which could indicate that it has a higher number of GCs, and a second peak in concentration between the two galaxies. The peak in GC candidate concentration between NGC 7332 and NGC 7339 could be an indication that these galaxies are interacting. However more statistical tests are needed to draw a final conclusion.

9. AREAS FOR FURTHER INVESTIGATION

To improve the outcomes of this project, the following sections describe additional steps and challenges that could be resolved given more time.

9.1. *Stacking more chips together*

The uiK_s diagram could be improved with a increased number of matched sources across the final images. Currently for the u and i band images only 2 of 36 total MegaCam chips were stacked together, which results in the number of matches limited by field of view of the current images. Increasing the number of chips staked together for the u and i band images would lead to more sources in the uiK_s diagram. Which would allow the diagram to more clearly show the separation of the the galaxies, stars, and GCs. Therefore initial selection of GC from the diagram would be more accurate. Larger images also reduce the risk of not encapsulating the whole GC systems around the galaxies.

9.2. *Magnitude vs. Flux radius plot*

Source-extractor outputs the magnitude and flux radius for every source in the images. The plot of magnitude versus flux radius identifies oversatureated stars, stars, and galaxies. As the GCs should be well defined point sources that are not unreasonably bright this plot could be used to further sort the GC candidates. As seen in Fig.9 the lower left region of GC candidates are more likely to by GC as they are not of too low in magnitude or too large in radius. The addition of this method would better sort the GC candidates.

9.3. *Further Galaxy and Star Culling*

To further separate galaxies from point sources (GCs, Stars) a point spread function (PSF) could be used to create a spread model over PSF magnitude graph Taylor et al. (2017) Fig.16. A PSF could be created on the images to account for atmospheric or optical distor-

tions by calculating the instruments response to a point source. Source extractor can then output a parameter called spread model using Eq.C1, the value of spread model for point sources has been shown to be in the range Eq.C2, as demonstrated by Desai et al. (2012). This effectively sorts galaxies from point sources.

To further separate stars from GCs using data from the CADC a $u'r'z'$ diagram could be created Taylor et al. (2017). The $u'r'z'$ diagram takes the magnitudes of sources in the u', r', and z' filters to sort out GCs based on their $(u'-r')_0$ and $(r'-z')_0$ colours as seen in Fig.17.

The redshift could also be determined for each GC candidate, sources with a comparably radial velocity to NGC 7332 or NGC 7339 would be more likely to be GCs Muñoz et al. (2014) however there is not the required data to implement this method.

9.4. *Source-Extractor, Scamp, and SWarp*

The programs Source-Extractor, Scamp, and SWarp perform better stacking, alignment, and photometry then Mira. Overcoming to the issues as discussed in section 3.2.1 would allow for increased number of matched sources and more accurate photometry leading to better GC identification with the uiK_s diagram and GC density analysis.

9.5. *Further GC density analysis*

To show the galaxies interaction though statistical analysis the Kolmogorov–Smirnov (K-S) test could be used as shown by Press & Teukolsky (1988). The K-S test can be applied on two dimensional data such as the RA/Dec distribution of GC candidates. This method assesses whether the distribution of globular clusters is consistent with a specific probability distribution or another data set. Therefore, it can be used to determine the likelihood that the GC distribution around these two galaxies deviates from the typical distribution of non-interacting spiral galaxies, aligning more closely with a expected distribution for interacting galaxies.

10. SUMMARY

To achieve the goal of locating globular clusters a application was made to CFHT to collect K_s band data on NGC 7332 and NGC 7339, in order to create a uiK_s colour colour diagram. After staking the images for the u, i, and K_s filters they were calibrated in RA/Dec and photometrically. Photometry was then performed on the images using Source-Extractor to gather the magnitudes and locations of sources in each image. Fallowing the uiK_s diagram method the globular clusters were located and sorted to find 90 GC candidates around the galaxies. The spacial distribution of the GCs was then studied to show an increased concentration of GC candidates between the two galaxies indicating the possibility they are in the early stages of interaction. However in order to make a determination more substantial statistical tests and photometry need to be done.

APPENDIX

A. FIGURES

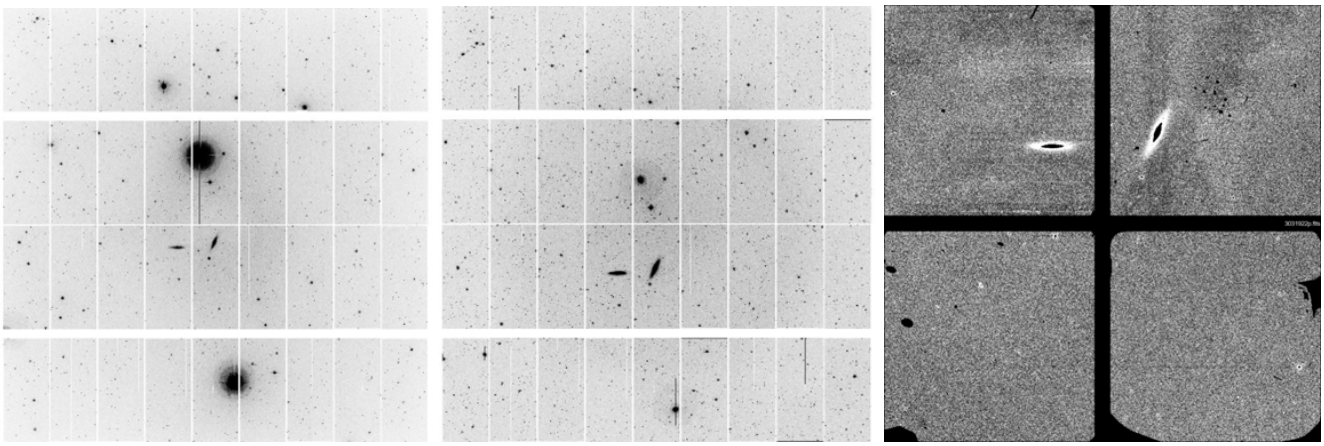

Figure 1. The pre-processed images from CFHT. (left) Detrended and Sky subtracted u Band image taken by CFHT's MegaCam instrument. (middle) Detrended and Sky subtracted i Band image taken by CFHT's MegaCam instrument. (right) Detrended and Sky subtracted K_s Band image taken by CFHT's WIRCam instrument.

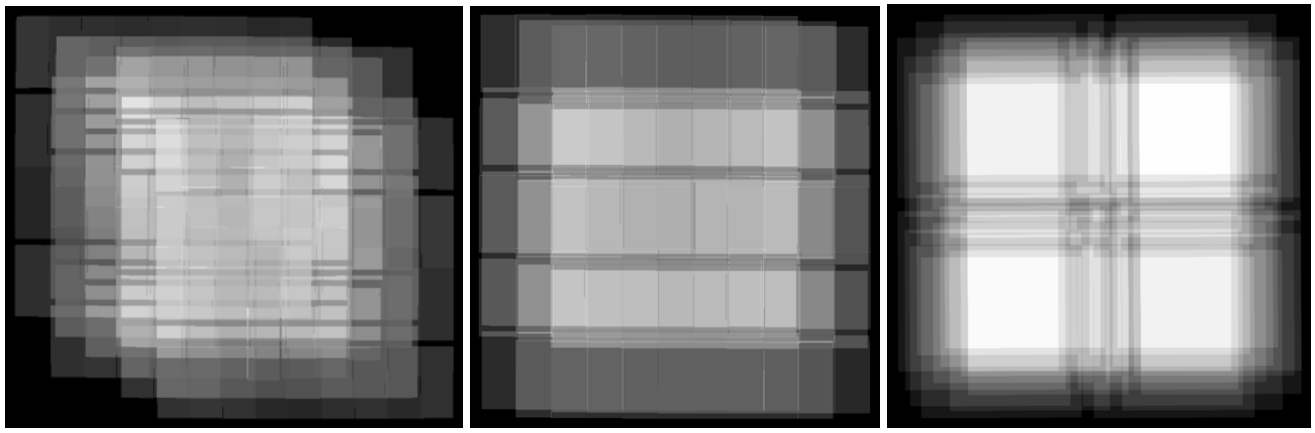

Figure 2. (left) dithering patter CFHT while the u band data was taken. (middle) dithering patter CFHT while the i band data was taken. (right) dithering patter CFHT while the K_s band data was taken. The dithering patterns of these observations are crucial as the near-IR sky changes on near seconds time scales, it affects the size of the final image, and the amount of overlap of the chips affecting the image stacking process.

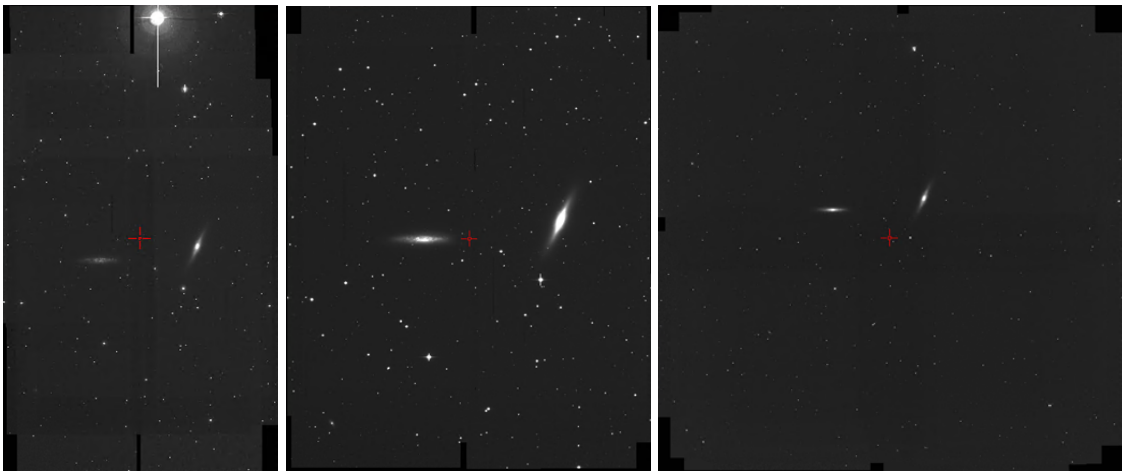

Figure 3. (left) final stacked u image made with 7 images using 2/36 Megacam chips stacked together using Mira. (middle) final stacked i image made with 6 images using 2/36 Megacam chips stacked together using Mira. (right) final stacked K_s image made with 121 images using 4/4 WIRCam chips stacked together using Mira.

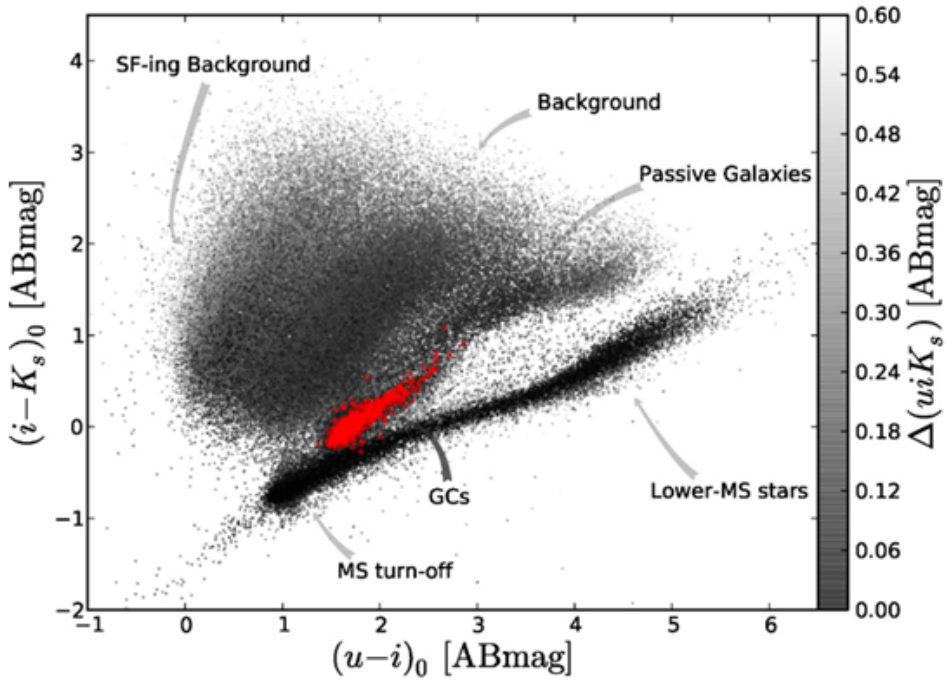

Figure 4. The uiK_s colour-colour diagram characterizing sources using magnitude measurements in the Virgo cluster Muñoz et al. (2014). Using the normalized colours $(u-i)_0$ and $(i-K_s)_0$ globular clusters can be separated from background galaxies an foreground stars. The red points marks indicate spectroscopically confirmed globular clusters. The colour bar indicates the total photometric error in magnitude measurements by Source-Extractor in each filter.

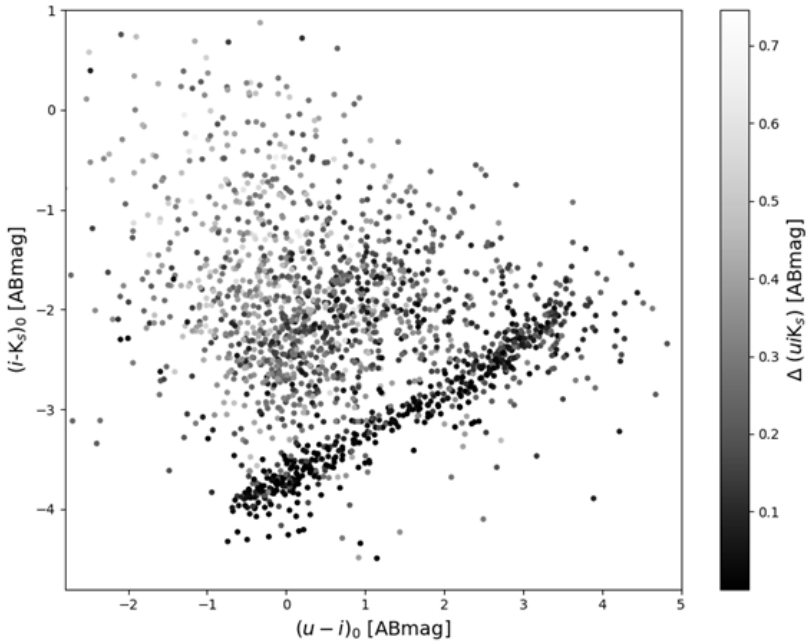

Figure 5. The uiK_s colour-colour diagram characterizing objects using magnitude measurements of sources around NGC 7332 and NCG 7339. Using the normalized colours $(u-i)_0$ and $(i-K_s)_0$ globular clusters can be separated from background galaxies and foreground stars as shown by Muñoz et al. (2014). The colour bar indicates the total photometric error in magnitude measurements by Source-Extractor in each filter.

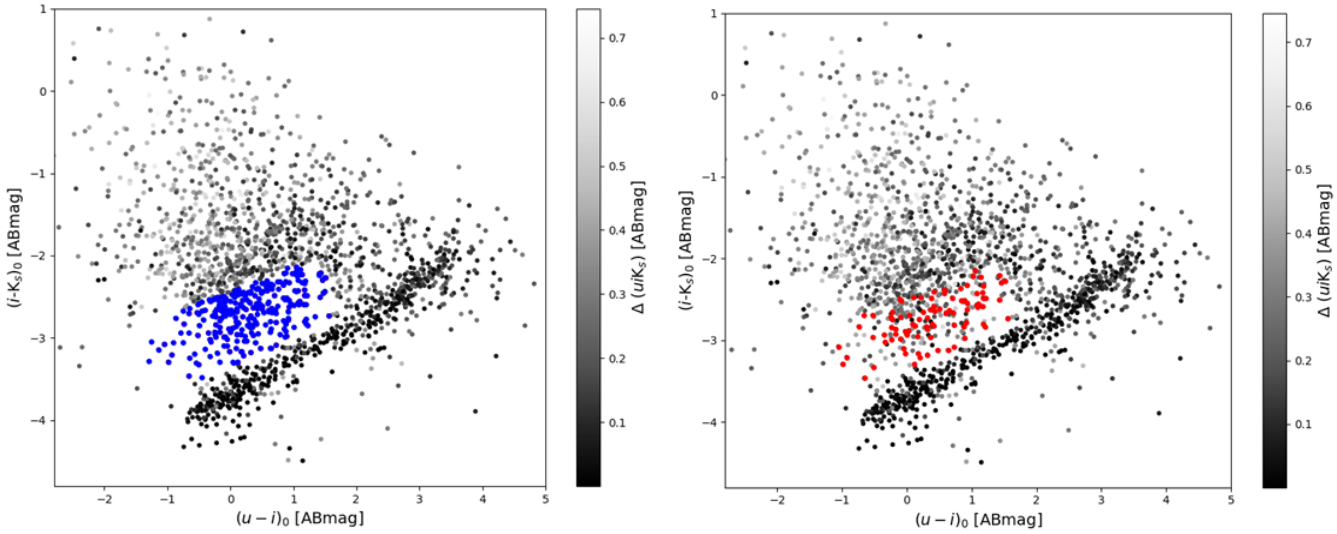

Figure 6. The uiK_s colour-colour diagram characterizing objects using magnitude measurements of sources around NGC 7332 and NCG 7339. The colour bar indicates the total photometric error in magnitude measurements by Source-Extractor in each filter. (left) The blue marks show the initial 282 sources selected as possible globular cluster candidates based on their location in the uiK_s diagram. (right) The red marks show 90 globular cluster candidates that have been sorted through using ellipticity.

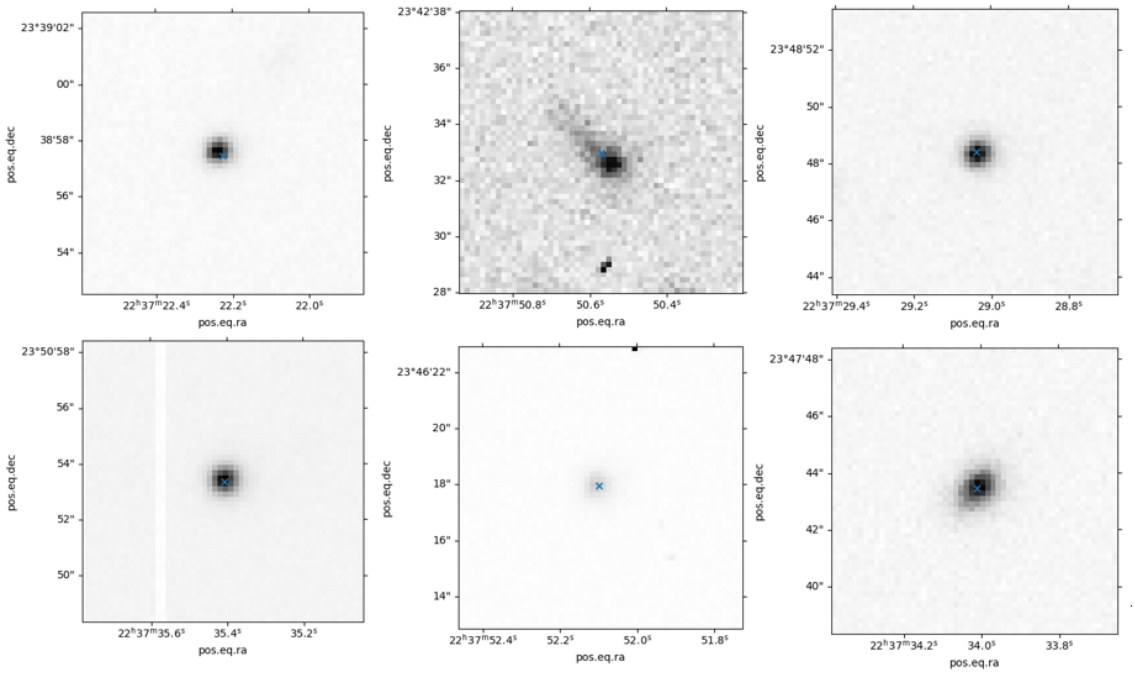

Figure 7. To assess the 282 initial globular cluster candidates, 10-arcsecond square cutouts were generated from the i-band image around each source. Ideally globular cluster candidates appear as well-defined point sources with low ellipticity. These example cutouts are characteristic of globular clusters.

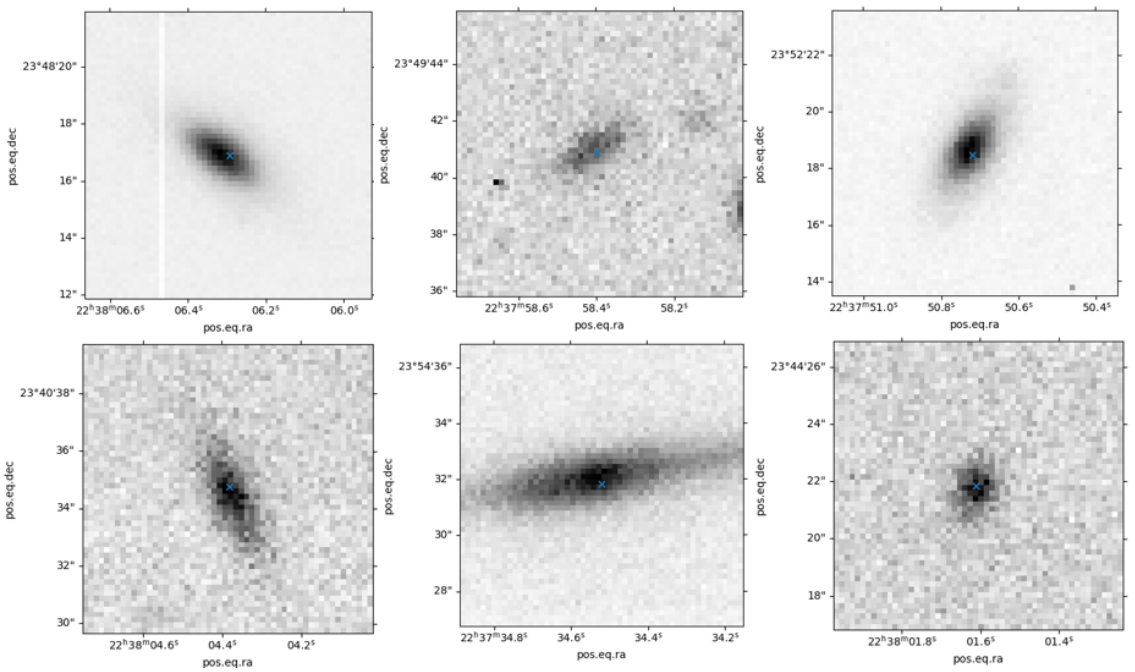

Figure 8. To assess the 282 initial globular cluster candidates, 10-arcsecond square cutouts were generated from the i-band image around each source. These example cutouts are un-characteristic of globular clusters they are less defined more elliptical sources. Therefore these sources are no longer considered globular cluster candidates.

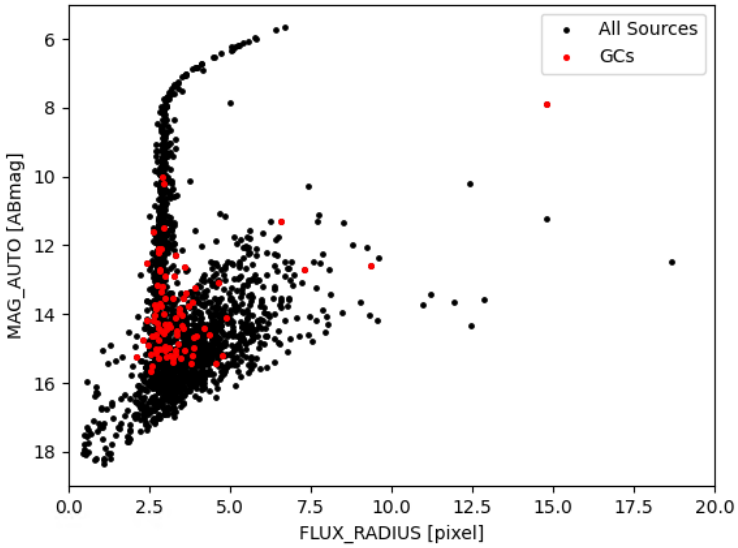

Figure 9. Plot of sources measured magnitudes in the i band versus their flux radius in pixels, the black marks show all 1928 sources, the red marks show the 90 globular cluster candidates. The top portion of the plot shows the oversatureated stars, the middle shows bright point sources which are foreground stars, the lower region shows extended fainter sources which are background galaxies.

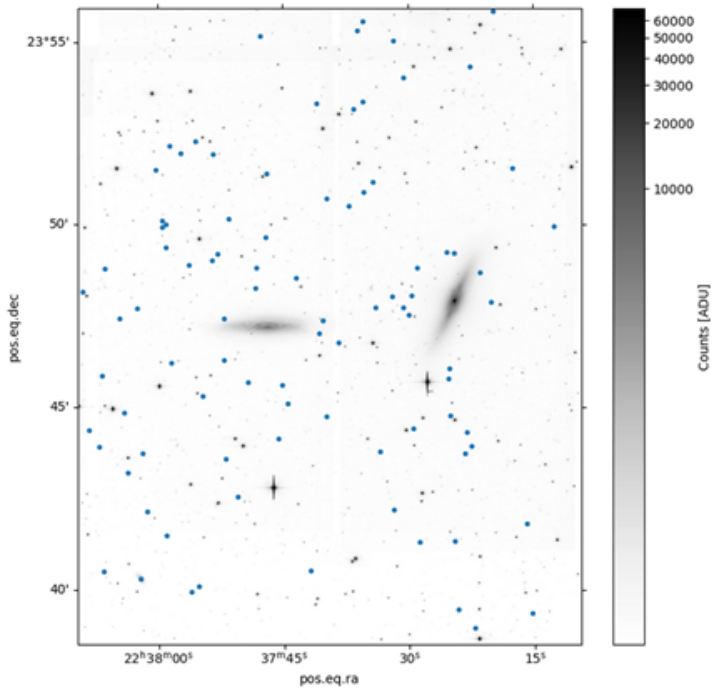

Figure 10. Plot of the i band image of NGC 7332 and NGC 7339 where the colour bar shows the counts at each RA/Dec location and the blue circles show the locations of the 90 globular cluster candidates.

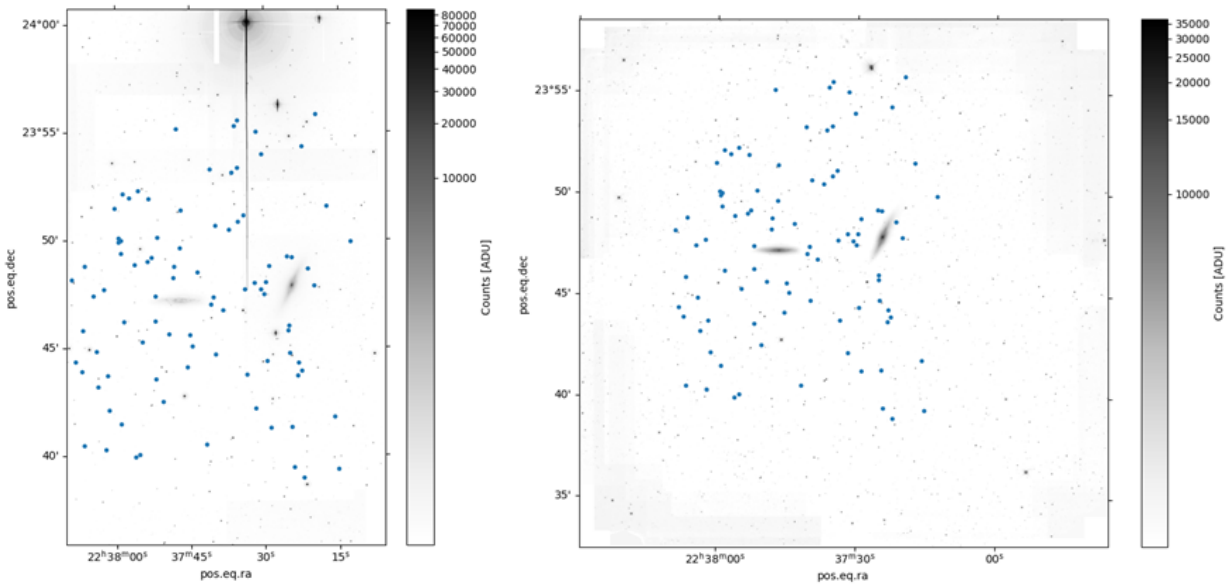

Figure 11. Plot of the u band image (left) and K_s band image (right) of NGC 7332 and NGC 7339 where the colour bar shows the counts at each RA/Dec location and the blue circles show the locations of the 90 globular cluster candidates.

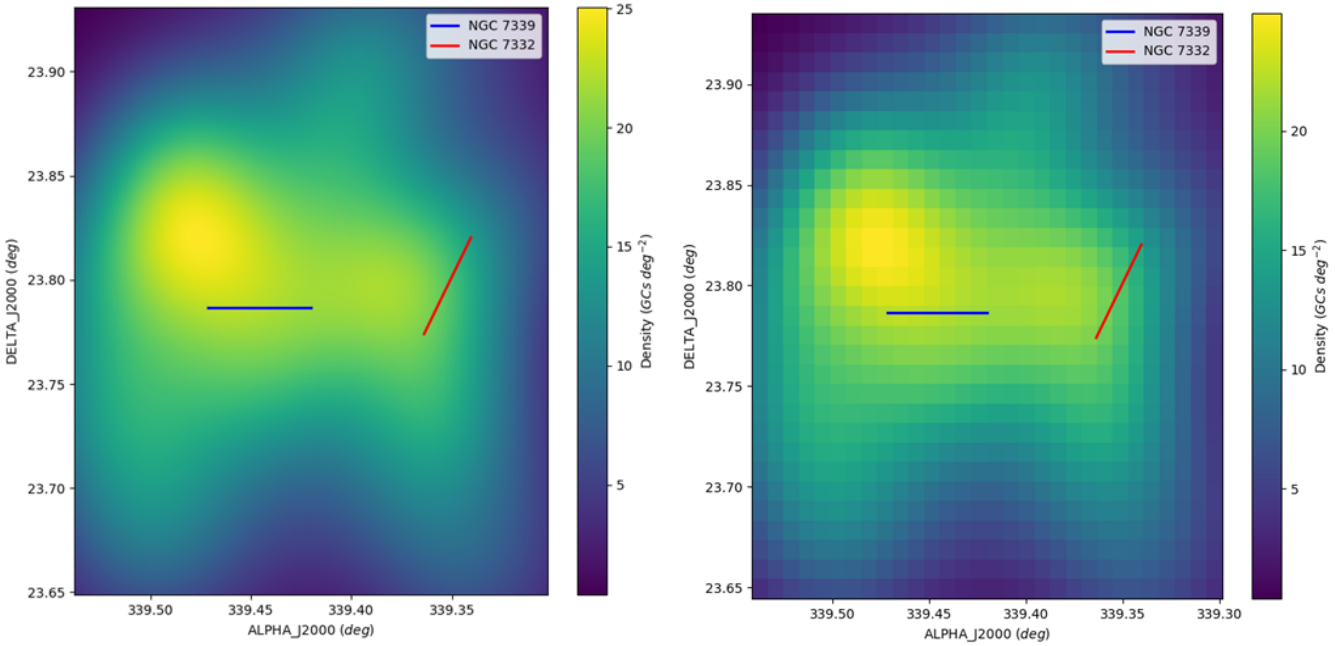

Figure 12. Plot of globular cluster candidate density using the Gaussian_kde Python module form Scipy.stats Virtanen et al. (2020). It works by splitting the plotting area into 300 bins on the left or 30 bins on the right then each globular cluster candidate adds weight to the thee bin it falls in. The density plot is then created by fitting a Gaussian curve to the weights and plotting using a colour gradient.

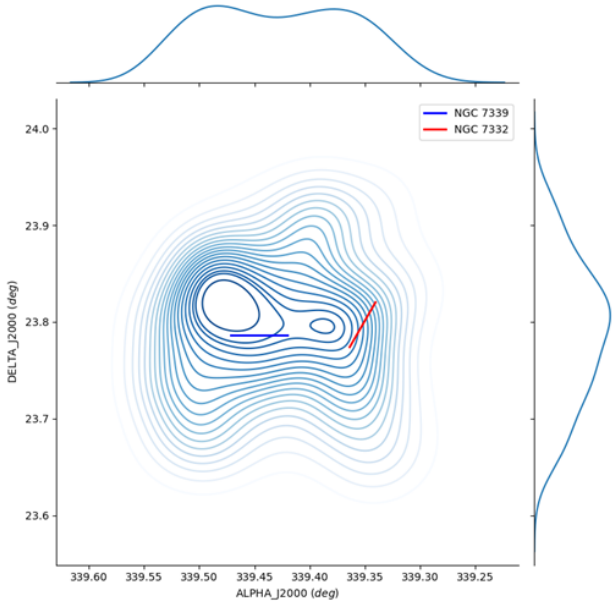

Figure 13. Plot of globular cluster candidate density using the Seaborn Waskom et al. (2017) Python package. It works by splitting the plotting area into 300 bins then each globular cluster candidate adds weight to the thee bin it falls in. The density plot is then created by fitting a Gaussian curve to the weights and plotting using a topographical map. On each axis there is the addition of a line graph showing the amount of globular clusters in each column/row of bins.

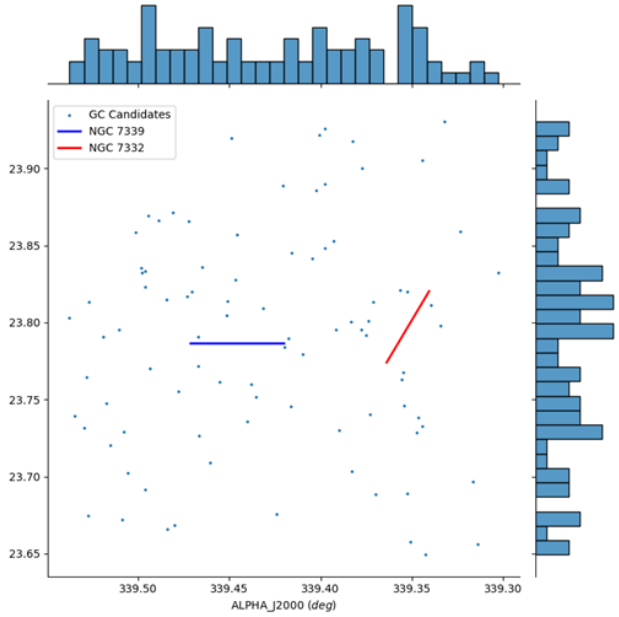

Figure 14. Plot of globular cluster candidate density using the Seaborn Waskom et al. (2017) Python package. It works by splitting the plotting area into 30 bins then on each axis a bar graph is created showing the amount of globular clusters in each column/row of bins. Then plots the RA/Dec positions of the globular cluster candidates as a scatter plot. This visualizes density by showing the columns/rows of bins containing the most candidates.

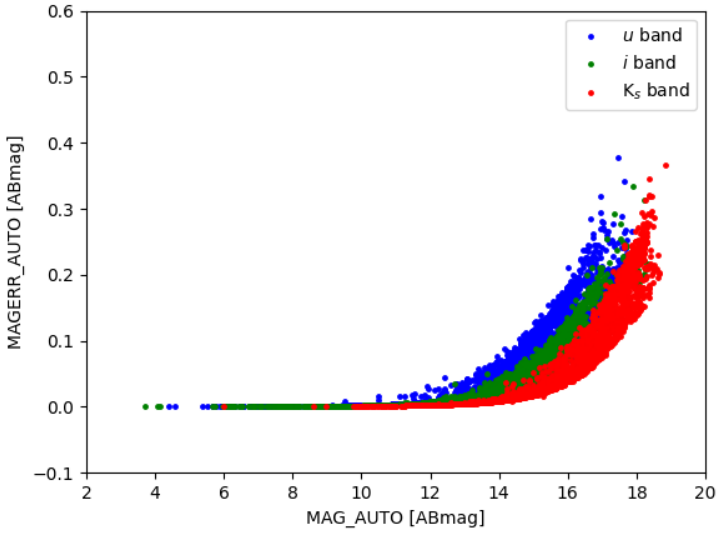

Figure 15. Plot of the magnitude measured for each source versus the rms error calculated by Source-Extractor for the u,i, and K_s filters. The graph shows constantly that the brightest objects have ~ 0 magnitudes error while dimmer objects have a maximum error of ~ 0.35 magnitudes.

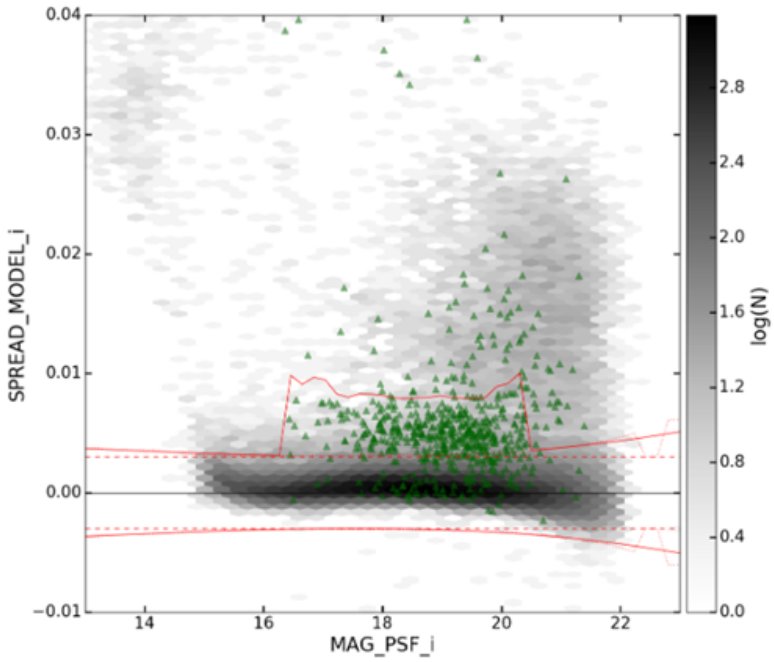

Figure 16. Galaxy-point source classification diagram for sources in the Virgo cluster as described in Taylor et al. (2017). The colour bar shows the logarithmic number density of sources. Green triangles show spectroscopically confirmed globular clusters. The 'Spread Model' parameter, calculated using Eq.C1, is a value output by Source-Extractor. The red lines outlining the region where the Spread Model value satisfies Eq.C2, indicating a point source rather than a galaxy, as demonstrated by Desai et al. (2012).

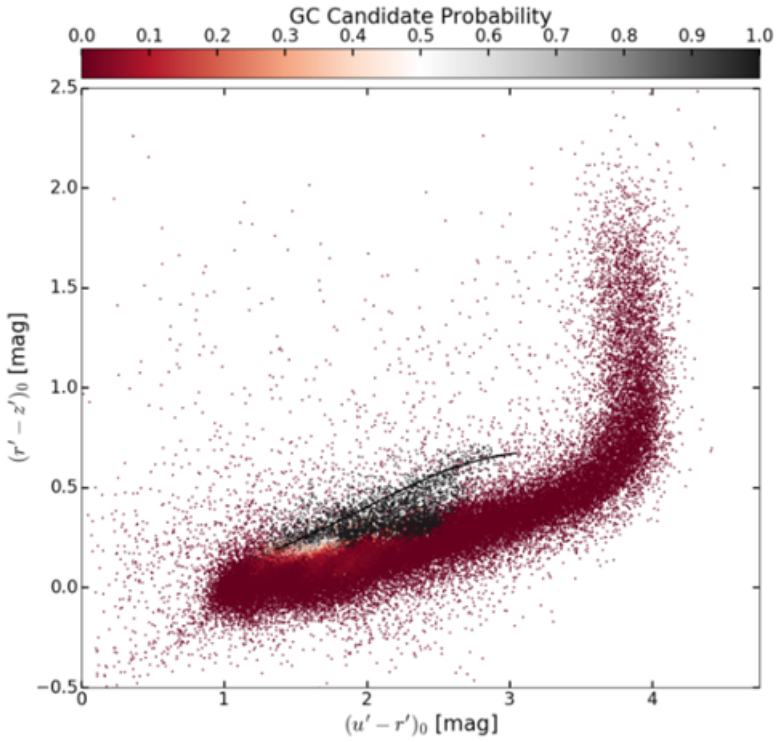

Figure 17. The $u'r'z'$ diagram showing probabilities of point sources to bye globular clusters in the Virgo cluster as described in Taylor et al. (2017). The colour bar illustrates the probability a source is a globular cluster with $P(GC) \approx 1.0$ around the black curve.

B. TABLES

Table 1. Relevant information to zeropoint calibration for each filter, the number of standard stars used in Mira, the zeropoint CFHT lists for 1 airmass, and the zeropoint Mira calculated.

Filter	u	i	K_s
Number standard star	7 Quasars	6 Quasars	20 Stars
ZP_{CFHT} [Vega mag]	25.26	25.70	24.43
ZP_{Mira} [Vega mag]	24.0575 ± 0.3201	24.0575 ± 0.2498	23.7193 ± 0.1006

C. EQUATIONS

Eq.C1 is the equation for SPREAD_MODEL used by Source-Extractor Taylor et al. (2017). The equation uses the local point source function (PSF), Φ, x is the image vector centred on the source, and G is the more extended model.

$$SPREAD\_MODEL = \frac{\Phi^T x}{\Phi^T \Phi} - \frac{G^T x}{G^T \Phi} \tag{C1}$$

Eq.C2 shows the definition used for point sources in the galaxy-point source diagram in Fig.16. Meaning sources with a SPREAD_MODEL value in the range described by Eq.C2 are more point source like, which separates them form background galaxies.

$$SPREAD\_MODEL = 0.0 \pm (0.003 + SPREADERR\_MODEL) \tag{C2}$$

REFERENCES

Albareti, F. D., Allende Prieto, C., Almeida, A., et al. 2017, ApJS, 233, 25, doi: 10.3847/1538-4365/aa8992

Barrick. 2024, Wircam Filters. https://www.cfht.hawaii.edu/Instruments/Filters/wircam.html

Bertin. 2024, MegaPrime Current Filter Characteristics. https://www.cfht.hawaii.edu/Instruments/Imaging/Megacam/specsinformation.html

Bertin, E. 2006, in Astronomical Society of the Pacific Conference Series, Vol. 351, Astronomical Data Analysis Software and Systems XV, ed. C. Gabriel, C. Arviset, D. Ponz, & S. Enrique, 112

Bertin, E., & Arnouts, S. 1996, A&AS, 117, 393, doi: 10.1051/aas:1996164

Bertin, E., Mellier, Y., Radovich, M., et al. 2002, in Astronomical Society of the Pacific Conference Series, Vol. 281, Astronomical Data Analysis Software and Systems XI, ed. D. A. Bohlender, D. Durand, & T. H. Handley, 228

Brodie, J. P., & Strader, J. 2006, ARA&A, 44, 193, doi: 10.1146/annurev.astro.44.051905.092441

Desai, S., Armstrong, R., Mohr, J. J., et al. 2012, ApJ, 757, 83, doi: 10.1088/0004-637X/757/1/83

Gaia Collaboration, Vallenari, A., Brown, A. G. A., et al. 2023, A&A, 674, A1, doi: 10.1051/0004-6361/202243940

Harris, W. E., & van den Bergh, S. 1981, AJ, 86, 1627, doi: 10.1086/113047

Helou, G., Madore, B. F., Schmitz, M., et al. 1991, in Astrophysics and Space Science Library, Vol. 171, Databases and On-line Data in Astronomy, ed. M. A. Albrecht & D. Egret, 89–106, doi: 10.1007/978-94-011-3250-3_10

Lang, D., Hogg, D. W., Mierle, K., Blanton, M., & Roweis, S. 2012, Astrometry.net: Astrometric calibration of images, Astrophysics Source Code Library, record ascl:1208.001

Mirametrics. 2024, Mira Pro x64. https://mirametrics.com

Muñoz, R. P., Puzia, T. H., Lançon, A., et al. 2014, ApJS, 210, 4, doi: 10.1088/0067-0049/210/1/4

Press, W. H., & Teukolsky, S. A. 1988, Computer in Physics, 2, 74, doi: 10.1063/1.4822753

Skrutskie, M. F., Cutri, R. M., Stiening, R., et al. 2006, The Astronomical Journal, 131, 1163, doi: 10.1086/498708

Taylor, M. 2011, TOPCAT: Tool for OPerations on Catalogues And Tables, Astrophysics Source Code Library, record ascl:1101.010

Taylor, M. A., Puzia, T. H., Muñoz, R. P., et al. 2017, MNRAS, 469, 3444, doi: 10.1093/mnras/stx1021

Virtanen, P., Gommers, R., Oliphant, T. E., et al. 2020, Nature Methods, 17, 261, doi: 10.1038/s41592-019-0686-2

Waskom, M., Botvinnik, O., O'Kane, D., et al. 2017, mwaskom/seaborn: v0.8.1 (September 2017), v0.8.1, Zenodo, doi: 10.5281/zenodo.883859

Wenger, M., Ochsenbein, F., Egret, D., et al. 2000, A&AS, 143, 9, doi: 10.1051/aas:2000332

Wicenec, A. J. 1997, in Astronomical Society of the Pacific Conference Series, Vol. 125, Astronomical Data Analysis Software and Systems VI, ed. G. Hunt & H. Payne, 278

Young, M. D., Dowell, J. L., & Rhode, K. L. 2012, AJ, 144, 103, doi: 10.1088/0004-6256/144/4/103